Melting of Peridotite to 140 Gigapascals

G. Fiquet, *et al.*

Science **329**, 1516 (2010);
DOI: 10.1126/science.1192448

21. O. Möhler, P. J. DeMott, G. Vali, Z. Levin, *Biogeosciences* **4**, 1059 (2007).
22. B. C. Christner, C. E. Morris, C. M. Foreman, R. M. Cai, D. C. Sands, *Science* **319**, 1214 (2008).
23. R. M. Bowers *et al.*, *Appl. Environ. Microbiol.* **75**, 5121 (2009).
24. K. A. Pratt *et al.*, *Nat. Geosci.* **2**, 398 (2009).
25. M. O. Andreae *et al.*, *Science* **303**, 1337 (2004).
26. P. Reutter *et al.*, *Atmos. Chem. Phys.* **9**, 7067 (2009).
27. M. Kulmala *et al.*, *J. Aerosol Sci.* **35**, 143 (2004).
28. J. Merikanto, D. V. Spracklen, G. W. Mann, S. J. Pickering, K. S. Carslaw, *Atmos. Chem. Phys.* **9**, 8601 (2009).
29. R. Krejci *et al.*, *Atmos. Chem. Phys.* **5**, 1527 (2005).
30. A. M. L. Ekman *et al.*, *Geophys. Res. Lett.* **35**, L17810 (2008).
31. U. Kuhn *et al.*, *Atmos. Chem. Phys.* **7**, 2855 (2007).
32. J. Lelieveld *et al.*, *Nature* **452**, 737 (2008).

33. Support from a large number of colleagues, agencies, and institutions is gratefully acknowledged as detailed in the supporting online material.

Supporting Online Material
www.sciencemag.org/cgi/content/full/329/5998/1513/DC1
Materials and Methods
SOM Text
Fig. S1
Tables S1 to S6
References and Notes

19 April 2010; accepted 28 June 2010
10.1126/science.1191056

Melting of Peridotite to 140 Gigapascals

G. Fiquet,[1]* A. L. Auzende,[1] J. Siebert,[1] A. Corgne,[2,3] H. Bureau,[1] H. Ozawa,[1,4] G. Garbarino[5]

Interrogating physical processes that occur within the lowermost mantle is a key to understanding Earth's evolution and present-day inner composition. Among such processes, partial melting has been proposed to explain mantle regions with ultralow seismic velocities near the core-mantle boundary, but experimental validation at the appropriate temperature and pressure regimes remains challenging. Using laser-heated diamond anvil cells, we constructed the solidus curve of a natural fertile peridotite between 36 and 140 gigapascals. Melting at core-mantle boundary pressures occurs at 4180 ± 150 kelvin, which is a value that matches estimated mantle geotherms. Molten regions may therefore exist at the base of the present-day mantle. Melting phase relations and element partitioning data also show that these liquids could host many incompatible elements at the base of the mantle.

Geophysical and geochemical observations favor the presence of chemical heterogeneities in the lowermost mantle. These are thought to be either primitive mantle residues (*1*), dense subducted slab components (*2*), products of chemical interactions between the core and mantle (*3*, *4*), or dense melts perhaps as old as the Earth itself (*5*). The core-mantle boundary is a complex region that has been the focus of numerous geophysical studies. Seismologic studies suggest the presence of two large low-shear velocity provinces (LLSVPs) under the African continent and in the pacific basin (*6*, *7*). The consensus view is that these slow regions (which are possibly up to 1000 km thick) exhibit an anomalously low shear velocity and increased bulk modulus but are not usually thought to be partially molten (*8*). Additionally, extensively documented ultralow-velocity zones (ULVZs) correspond to localized features at the core mantle boundary (CMB), with strong reductions in seismic velocities (in the range of 10 to 30%) for both P and S waves (*9*, *10*); the interpretation is that these zones may be partially molten (*5*). Recent high-resolution waveform studies also find evidence that the ULVZ material is denser than the surrounding mantle (*11*). These partially molten regions have not been detected to be laterally continuous and have a thickness ranging from a few kilometers up to about 50 km.

It is attractive to link these observations with an episode of extensive melting that probably affected the primitive Earth, leading to the formation of a deep magma ocean. If the evolution of a terrestrial magma ocean resulted in the formation of a layer of melt at the base of the mantle early in Earth history, its survival depends on whether it was (and maybe still is) gravitationally and chemically stable (*12*). If this is the case, such a layer would be an ideal candidate for an unsampled geochemical reservoir hosting a variety of incompatible species, notably the planet's missing budget of heat-producing elements (*13*). The presence of high-pressure melts would also have consequences for chemical reactions between the mantle and core, the dynamics of the lowermost mantle, and the heat flow across the CMB.

To constrain the existence of melt at the base of the mantle, we performed melting experiments on a fertile peridotite composition over a range of lower-mantle pressures between 36 and 140 GPa using a laser-heated diamond-anvil cell (DAC) coupled with in situ synchrotron measurements (*14*). Our study thus extends the pressure range of previous measurements (*15*, *16*) of the solidus and liquidus temperatures of a mantle-like composition to depths exceeding those of the CMB at 2900 km. The starting material used for the high-pressure high-temperature melting experiments is a natural KLB-1 peridotite (*14*). To ensure chemical homogeneity at the smallest scale and Fe as mostly Fe^{2+}, a glass was prepared by using an aerodynamic levitation device coupled with CO_2 laser heating under slightly reducing conditions of oxygen fugacity (*17*). At high temperature, pressures were measured from cell parameters of the magnesium perovskite $(Mg,Fe)SiO_3$ by using a thermal equation of state recently reported for the same KLB-1 peridotitic starting material as

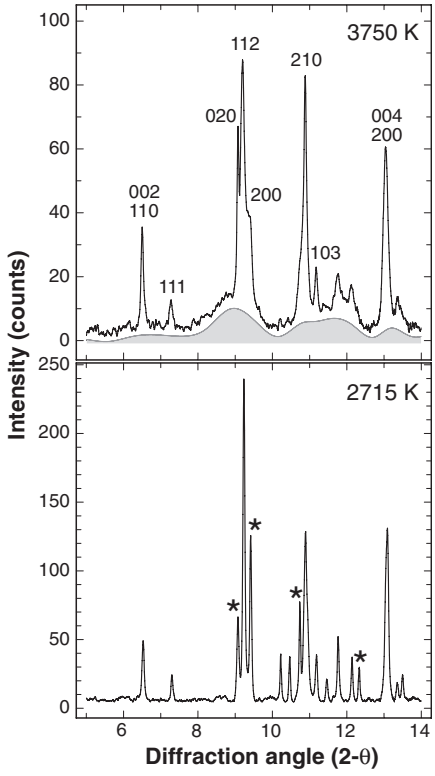

Fig. 1. Diffraction patterns collected at 61 GPa after normalized reference background subtraction: subsolidus at 2715 K (**bottom**) and above solidus at 3750 K (**top**). The diffuse scattering liquid contribution is outlined by the shaded area as a guide; it does not correspond to a physical structural model of the liquid. HKL indexes are given for remaining diffraction peaks that can be assigned to magnesium silicate perovskite, observed above the solidus temperature at this pressure (top). Stars denote diffraction peaks of Ca-perovskite and ferropericlase affected by partial melting at these conditions (bottom).

[1]Institut de Minéralogie et de Physique des Milieux Condensés, Institut de Physique du Globe de Paris, Université Pierre et Marie Curie, UMR CNRS 7590, Université Paris Diderot, 140 rue de Lourmel, 75015 Paris, France. [2]Institut de Physique du Globe de Paris, Equipe de Minéralogie à l'Institut de Minéralogie et de Physique des Milieux Condensés, 140 rue de Lourmel, 75015 Paris, France. [3]Observatoire Midi-Pyrénées, UMR CNRS 5562, 14 rue Edouard Belin, 31400 Toulouse, France. [4]Department of Earth and Planetary Sciences, Tokyo Institute of Technology 2-12-1 Ookayama, Meguro-ku, Tokyo 152-8551, Japan. [5]European Synchrotron Radiation Facility, BP220, 38043 Grenoble cedex, France.

*To whom correspondence should be addressed. E-mail: guillame.fiquet@impmc.upmc.fr

used in our study (*18*). We used in situ x-ray diffraction as primary criterion for melting (*19*) and to determine the order in which crystalline phases melt (Fig. 1).

At 36 GPa, melting begins at 2800 K, with Mg- and Ca-perovskite ($CaSiO_3$) melting first. The produced melt is far more laser-absorbent; a sharp increase in temperature accompanies melting. This leads almost instantly to conditions above the liquidus, preventing an accurate characterization of a detailed melting sequence. Transmission electron microscopy (TEM) examination of a focused ion beam section made across the laser-heated spot on the recovered sample (fig. S3) and the large temperature increase at melting may indicate that Mg-perovskite melts early in the sequence (fig. S4). At this pressure, the liquidus temperature is ~3850 K, as determined during cooling from a fully molten state by a large temperature drop when the first phase crystallizes. At 61 GPa, melting of ferropericlase (Mg,Fe)O indicates the solidus temperature is ~3050 K, closely followed by melting of Ca-perovskite with increasing temperature. Mg-perovskite is the last stable phase below the liquidus, which is ~4200 K. The observation of the recovered sample (Fig. 2) reveals the presence of connected veins of ferropericlase in a matrix made of Mg-perovskite. Ca-perovskite grains are found along these veins as well as within the Mg-perovskite matrix, suggesting that Ca-perovskite was partly mobilized by melting. Ferropericlase veins also collected small (<100 nm) globules of metallic iron, which is consistent with the disproportionation of ferrous iron in the stability field of Mg-perovskite (*20*). At pressures above 61 GPa, it is more difficult to distinguish whether ferropericlase or Ca-perovskite melts first. It is clear, however, that Mg-perovskite is the last solid phase below the liquidus. We observed a smooth increase of melting temperatures with increasing pressures. At 112 GPa, the solidus is located at 3910 K. At CMB pressure and temperature conditions (136 GPa and temperatures above 4000 K) and above, the melting sequence remains the same: Ca-perovskite and ferropericlase melt first, followed by Mg-perovskite. Mg-perovskite is thus the liquidus phase between 60 GPa (perhaps less) and pressure conditions at the CMB (fig. S5).

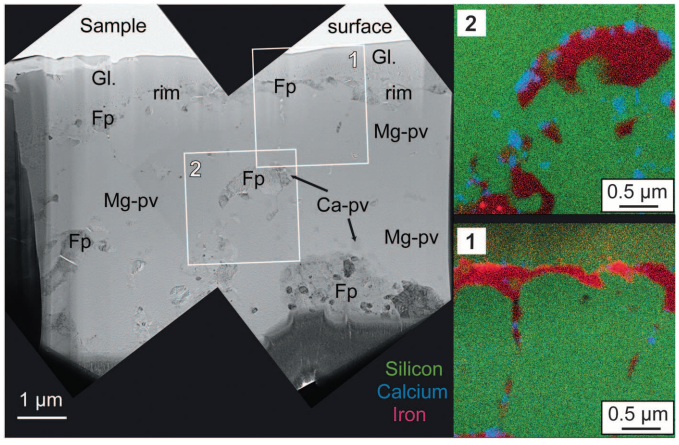

Fig. 2. Analytical TEM examination of a sample recovered after partial melting at 61 GPa: (left) bright field micrograph and (right) chemical maps. Some untransformed glassy material (Gl.) can be observed near the surface (panel 1), with chemical analysis yielding the average chemical composition of the starting material, thus showing the absence of reaction between sample and diamond during experimentation. A rim of ferropericlase (Fp) crystals appearing in red (iron-rich) exists at the edge of the laser-heated area. These crystals connect by veins to large patches of ferropericlase dispersed in the central area dominated by magnesium silicate perovskite (Mg-pv) in green (silicon-rich). Calcium silicate perovskite (Ca-pv) grains appear in blue (calcium-rich); most of them are located along ferropericlase-rich veins or at the edge of ferropericlase patches (panel 2). Some metallic iron precipitates exist in the iron-enriched ferropericlase regions (bright red spots). Melts probably formed after melting of ferropericlase and Ca-perovskite, which tend to percolate away from the heated area (probably as a result of thermal pressure) then crystallize on the edge in contact with the cold untransformed glassy material to form a rim surrounding the heated area.

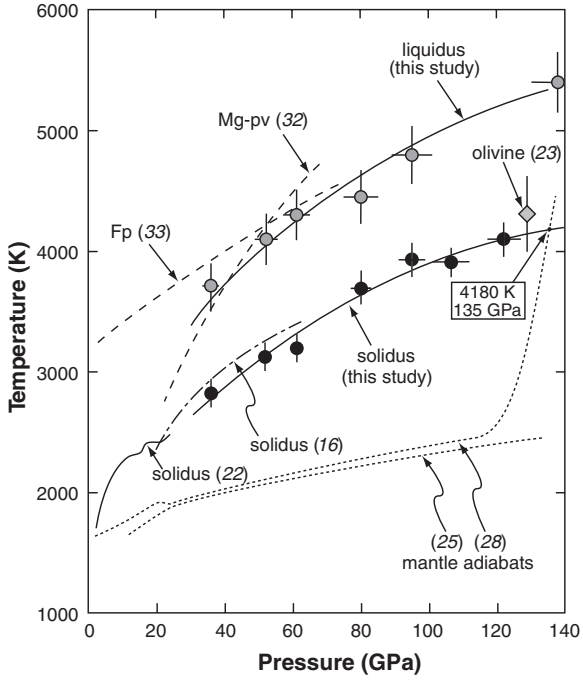

Fig. 3. Solidus (black solid circles) and liquidus (gray solid circles) of peridotite, along with melting curve data from the literature. Shown are the average estimate of the solidus for KLB-1 peridotite from previous multi-anvil work (*22*); the solid gray diamond indicates the shock melting point of olivine (*23*). Melting temperatures of the major lower mantle phases Mg-perovskite (*32*) and ferropericlase (*33*) are indicated by long-dashed lines. Melting data for a pyrolitic composition (dot-dashed line) are from (*16*). Temperature error bars represent temperature fluctuations during heating. Pressure error bars include the pressure variation in the sample chamber associated with temperature fluctuations as well as the uncertainty in the thermal equation of state of the magnesium silicate perovskite. Mantle geotherms are given for reference [adiabatic (*25*)] or estimated from perovskite to post-perovskite transition (*28*). Our solidus line, extrapolated to the CMB (solid line), intersects the geotherm at 135 GPa and 4180 K.

Above 61 GPa, the observed liquidus phase deviates from previous observations made at 24 GPa in multi-anvil experiments, in which ferropericlase was shown to be the liquidus phase, followed by Mg-perovskite 50 K below the liquidus (located at 2600 K) and Ca-perovskite 150 K lower, near the solidus (*21*). However, our observations are in qualitative agreement with other multi-anvil experiments (*15*), which suggest that Mg-perovskite should replace ferropericlase as the liquidus phase at pressures above 30 GPa, whereas our measurements suggest that this should happen at pressures above 36 GPa.

Solidus and liquidus points determined in this study compare well with literature data (Fig. 3). Data from previous DAC work in the 40 to 60 GPa range (*16*) are reported as an average solidus curve derived from the last subsolidus measurements and the appearance of first melt described in this study. Our measurements are in agreement with this work, although a completely different melting criterion was used in the latter study. Extrapolation of our solidus curve to lower pressures is also consistent with a large-volume press measurement of the solidus for KLB-1 peridotite (*22*). Furthermore, our data are also in good agreement with the mantle solidus inferred at CMB conditions from a single shock experiment on $(Mg_{0.9},Fe_{0.1})_2SiO_4$ (*23*) and from recent first principles molecular dynamics simulations (*24*). In the latter study, the predicted melting temperature of $MgSiO_3$ perovskite at 136 GPa is 5400 ± 600 K, and the authors estimate a mantle solidus temperature of 4100 K.

The solidus curve is about 1400 K above an average mantle adiabat (*25*) at mid-mantle pressures, but the difference shrinks rapidly above 120 GPa as we approach the CMB (Fig. 3). At

135 GPa, the peridotitic mantle solidus temperature extrapolated from our data set is at 4180 ± 150 K. This value is within the range of proposed temperatures on the core side of the CMB, as calculated from an outer-core adiabat and melting experiments on iron alloys (*26*, *27*) or as constrained by the reverse transition from the $CaIrO_3$-type to the perovskite phase at the base of the D″ layer (*28*). Partial melting in the deepest part of the mantle is therefore highly plausible. This process could therefore explain the presence of ULVZs. The close match between the average geotherm and mantle solidus at the CMB may also explain why ULVZs are not observed as a continuous layer in the deep mantle, with thicknesses of partially molten regions varying dramatically from cold to hot mantle areas.

Our results also provide insights in the way an early magma ocean could have crystallized. Partial melting of mantle material and related fractional crystallization will have important geochemical implications in terms of trace elements. This applies for both the inventory of incompatible elements and the isotopic evolution of the Earth. For instance, the semiquantitative analysis made on the sample recovered from 61 GPa shows a clear enrichment of the ferropericlase in iron, and an ubiquitous iron depletion in Mg-perovskite (table S1), which is in agreement with observations made in earlier studies [(*26*) and references therein]. Partial melts enriched in Ca-perovskite and ferropericlase components are thus expected to be denser than a solid residue of Fe-depleted Mg-perovskite. These liquids could have segregated downward and remained at least partly isolated in the lower mantle if mantle convection was not too vigorous [(*29*) and references therein]. Because Ca-perovskite is the major host mineral for many key trace elements, such as U, Th, and rare earth elements (*30*), these liquids could fractionate and host at present many incompatible elements at the core-mantle boundary, thus offering an explanation for primordial chemical signatures at the base of the mantle.

The estimated thickness of such a partially molten layer varies between 0 to 35 km from the intersection of the modern geotherm shown in Fig. 3 with the solidus of the mantle silicate material obtained in our study; however, this thickness could have been as large as 100 km in the Archean, assuming a secular cooling proceeding at a maximum rate of 100 K per billion years (*31*). These features depend on the estimates of the geotherm in the CMB region, which depends on the core thermal profile and temperature. The extension of such partially molten regions would also vary with lateral variations of the geotherm in the lowermost mantle, with the thickest portions occurring at the base of upwelling plumes and a thin layer elsewhere, which is compatible with seismic observations of ULVZs. Such a partially molten layer can alter several properties of the lowermost mantle that could, as proposed earlier (*5*), control the convection regime of the lowermost mantle and the heat transfer between core and mantle and affect the stability of the thermal boundary layer at the CMB.

References and Notes

1. L. H. Kellogg, B. H. Hager, R. D. van der Hilst, *Science* **283**, 1881 (1999).
2. F. Albarede, R. D. van der Hilst, *Philos. Trans. R. Soc. London. A* **360**, 2569 (2002).
3. A. D. Brandon, R. J. Walker, J. W. Morgan, M. D. Norman, H. M. Prichard, *Science* **280**, 1570 (1998).
4. D. J. Frost *et al.*, *J. Geophys. Res.* **115**, B02202 (2010).
5. Q. Williams, E. J. Garnero, *Science* **273**, 1528 (1996).
6. D. Helmberger, T. Lay, S. Ni, M. Gurnis, *Proc. Natl. Acad. Sci. U.S.A.* **102**, 17257 (2005).
7. E. J. Garnero, A. K. McNamara, *Science* **320**, 626 (2008).
8. T. Lay, E. J. Garnero, Q. Williams, *Phys. Earth Planet. Inter.* **146**, 441 (2004).
9. L. X. Wen, D. V. Helmberger, *J. Geophys. Res. Solid Earth* **103** (B8), 17901 (1998).
10. E. J. Garnero, D. V. Helmberger, *J. Geophys. Res. Solid Earth* **103**, 12495 (1998).
11. S. Rost, E. J. Garnero, Q. Williams, *J. Geophys. Res. Solid Earth* **111** (B09310), 1 (2006).
12. S. Labrosse, J. W. Hernlund, N. Coltice, *Nature* **450**, 866 (2007).
13. M. Boyet, R. W. Carlson, *Science* **309**, 576 (2005).
14. Materials and methods are available as supporting material on *Science* Online.
15. E. Ito, A. Kubo, T. Katsura, M. J. Walter, *Phys. Earth Planet. Inter.* **143–144**, 397 (2004).
16. A. Zerr, A. Diegeler, R. Boehler, *Science* **281**, 243 (1998).
17. L. Hennet *et al.*, *Rev. Sci. Instrum.* **73**, 124 (2002).
18. A. Ricolleau *et al.*, *Geophys. Res. Lett.* **36**, L06302 (2009).
19. A. Dewaele, M. Mezouar, N. Guignot, P. Loubeyre, *Phys. Rev. B* **76**, 144106 (2007).
20. D. J. Frost *et al.*, *Nature* **428**, 409 (2004).
21. R. G. Trønnes, D. J. Frost, *Earth Planet. Sci. Lett.* **197**, 117 (2002).
22. J. Zhang, C. Herzberg, *J. Geophys. Res.* **99**, 17729 (1994).
23. K. G. Holland, T. J. Ahrens, *Science* **275**, 1623 (1997).
24. L. Stixrude, N. de Koker, N. Sun, M. Mookherjee, B. B. Karki, *Earth Planet. Sci. Lett.* **278**, 226 (2009).
25. J. M. Brown, T. S. Shankland, *J. R. Astron. Soc.* **66**, 579 (1981).
26. R. Boehler, *Rev. Geophys.* **38**, 221 (2000).
27. Q. Williams, R. Jeanloz, *J. Geophys. Res.* **95**, 19299 (1990).
28. S. Ono, A. Oganov, *Earth Planet. Sci. Lett.* **236**, 914 (2005).
29. C.-T. Lee *et al.*, *Nature* **463**, 930 (2010).
30. A. Corgne, C. Liebske, B. J. Wood, D. C. Rubie, D. J. Frost, *Geochim. Cosmochim. Acta* **69**, 485 (2005).
31. C. Michaut, C. Jaupart, *Earth Planet. Sci. Lett.* **257**, 83 (2007), and references therein.

32. A. Zerr, R. Boehler, *Science* **262**, 553 (1993).
33. A. Zerr, R. Boehler, *Nature* **371**, 506 (1994).
34. We thank L. Hennet and G. Ona Nguema for experimental assistance. X-ray diffraction plots were made using DATLAB software developed by K. Syassen. A.L.A. acknowledges support from Institut National des Sciences de l'Univers (INSU) program "PNP, theme SEDI-TPS," and A.C. acknowledges support from the European Research Council (ERC) under the European Community's Seventh Framework Programme (FP7/2007-2013)/ERC grant agreement 207467. The Focused Ion Beam (FIB) and Scanning Electron Microscope (SEM) facility of the Institut de Minéralogie et de Physique des Milieux Condensés is supported by Région Ile de France grant SESAME 2006 N°I-07-593/R, INSU-CNRS, Institut de Physique (INP)–CNRS, University Pierre et Marie Curie–Paris 6, and by the French National Research Agency (ANR) grant ANR-07-BLAN-0124-01.

Supporting Online Material

www.sciencemag.org/cgi/content/full/329/5998/1516/DC1
Materials and Methods
Figs. S1 to S5
Table S1
References

18 May 2010; accepted 2 August 2010
10.1126/science.1192448

A Test of the Snowball Theory for the Rate of Evolution of Hybrid Incompatibilities

Daniel R. Matute, Ian A. Butler, David A. Turissini, Jerry A. Coyne

Hybrids between species are often sterile or inviable because the long-diverged genomes of their parents cause developmental problems when they come together in a single individual. According to the Dobzhansky-Muller (DM) model, the number of genes involved in these "intrinsic postzygotic incompatibilities" should increase faster than linearly with the divergence time between species. This straightforward prediction of the DM model has remained contentious owing to a lack of explicit tests. Examining two pairs of *Drosophila* species, we show that the number of genes involved in postzygotic isolation increases at least as fast as the square of the number of substitutions (an index of divergence time) between species. This observation verifies a key prediction of the DM model.

Biological speciation involves the evolution of barriers to gene flow between two populations (*1*, *2*). One of the most effective of those barriers, because it is considered irreversible, is "intrinsic postzygotic isolation," the developmentally based inviability or sterility of species hybrids. Dobzhansky (*1*) and Muller (*3*) proposed a simple two-locus model showing how this form of isolation can result from the accumulation of genes that function normally in a pure-species genome but produce epistatic interactions in hybrids.

The classic version of the Dobzhansky-Muller (DM) model, a population-genetics theory for the evolution of reproductive isolation (*2*), begins with

Department of Ecology and Evolution, The University of Chicago, 1101 East 57th Street, Chicago, IL 60637, USA.

*To whom correspondence should be addressed. E-mail: dmatute@uchicago.edu